Multipole induced splitting of metal-cage vibrations in crystalline endohedral D_{2d}-M_2@C_{84} dimetallofullerenes

M. Krause[a)]
Institut für Materialphysik, Universität Wien, Strudlhofgasse 4, A-1090 Wien, Austria and Leibniz-Institut für Festkörper- und Werkstofforschung Dresden, Helmholtzstr. 20, 01069 Dresden, Germany

V. N. Popov
Faculty of Physics, University of Sofia, 1164 Sofia, Bulgaria

M. Inakuma, N. Tagmatarchis,[b)] and H. Shinohara
Department of Chemistry, Nagoya University, Nagoya 464-8602, Japan

P. Georgi and L. Dunsch
Leibniz-Institut für Festkörper- und Werkstofforschung Dresden, Helmholtzstr. 20, 01069 Dresden, Germany

H. Kuzmany
Institut für Materialphysik, Universität Wien, Strudlhofgasse 4, A-1090 Wien, Austria

(Received 12 September 2003; accepted 20 October 2003)

Metal-carbon cage vibrations of crystalline endohedral D_{2d}-M_2@C_{84} (M=Sc,Y,Dy) dimetallofullerenes were analyzed by temperature dependent Raman scattering and a dynamical force field model. Three groups of metal-carbon cage modes were found at energies of 35–200 cm^{-1} and assigned to metal-cage stretching and deformation vibrations. They exhibit a textbook example for the splitting of molecular vibrations in a crystal field. Induced dipole–dipole and quadrupole–quadrupole interactions account quantitatively for the observed mode splitting. Based on the metal-cage vibrational structure it is demonstrated that D_{2d}-Y_2@C_{84} dimetallofullerene retains a monoclinic crystal structure up to 550 K and undergoes a transition from a disordered to an ordered orientational state at a temperature of approximately 150 K. © *2004 American Institute of Physics.*
[DOI: 10.1063/1.1632899]

I. INTRODUCTION

The encapsulation of atoms and small molecules has been one of the central objectives in fullerene research since its beginning.[1] Numerous metals, the noble gases, and the group 15 elements nitrogen and phosphorous were successfully encaged.[2–4] Scandium plays a special role, since metallofullerenes with up to four Sc atoms could be prepared. More recently fullerenes with four atomic heteronuclear encapsulates as Sc_3N (Ref. 5) and Sc_2C_2 (Ref. 6) were synthesized. Among the carbon cages the D_{2d}-C_{84} isomer No. 23 (Ref. 7) is of particular interest, as it exhibits an unique stability without as well as with different encapsulates like Sc_2 or Sc_2C_2. Hence the influence of the intrafullerene charge transfer on molecular and solid state properties can be studied. Due to the charge transfer from the endohedral species to the carbon cage larger dipole and quadrupole moments than for empty cages are expected. So far little is known on the influence of electrostatic interactions on the solid state properties of endohedral fullerenes. However they have to be taken into account in addition to van der Waals interactions which are the dominating forces in crystals of empty fullerenes.

Vibrational spectroscopy has been a key technique for the analysis of fullerenes in general. It allows for the determination of the C_{60} charge state in A_xC_{60} (A=K,Rb,Cs; x=0,1,3,4,6) alkaline metal fullerides, supplies experimental proof for dimer formation and gives evidence for the phase transition in solid C_{60}.[8] Studies of fullerenes beyond C_{60} suffer from the high number of cage modes, which makes a detailed mode analysis ambiguous or even impossible. The metal-cage modes however provide an excellent target for the analysis as they appear in a rather convenient frequency range between 200 and 35 cm^{-1}, well separated from lattice modes below 25 cm^{-1} on the one and cage modes above 200 cm^{-1} on the other hand. So far, metal-cage modes have been investigated mainly for monometallofullerenes. Such spectra always showed two lines which are Raman and IR active.[9–12] Recently, preliminary results were reported for metal-cage modes of dimetallofullerene D_{2d}-Sc_2@C_{84}.[13] In this case, unexpectedly many metal-cage lines appeared in the low frequency Raman spectrum. A similar large number of low energy modes was observed for crystalline Sc_3N@C_{80}.[14] Tentatively, crystal field and Davydov splitting of low energetic molecular vibrations were made responsible for these observations.

By analyzing temperature dependent Raman scattering of equistructural M_2@C_{84} dimetallofullerenes and applying a dynamical force field model we demonstrate in this paper that such system allows for a case study of crystal field and

[a)]Present address: Leibniz-Institut für Festkörper- und Werkstoffforschung Dresden, Helmholtzstr. 20, D-01069 Dresden, Germany.
[b)]Present address: Dipartimanto di Scienze Farmceutiche, Universita di Trieste, Piazzale Europa 1, I-34100 Trieste, Italy.

Davydov splitting. The latter mechanism is also known as factor group splitting. Here, M is one of the metals Sc, Y, or Dy and the fullerene cage is the D_{2d}-C_{84} isomer No. 23. The experiments revealed a set of metal dependent vibrational modes at wave numbers between 35–200 cm^{-1}. They displayed a pattern of three groups composed of up to four lines and were assigned to the stretching, antisymmetric and symmetric deformation modes of the encaged metals. For the detailed mode assignment, crystal field and factor group splittings were calculated using a dynamical force field model. As expected, the static crystal field shows the characteristics of a quadrupole–quadrupole interaction of the nondipolar $M_2@C_{84}$ molecules. Whenever a molecular dipole is induced during a metal-cage vibration as, e.g., for the antisymmetric M_2-C_{84} stretching mode, an induced dipole-induced dipole coupling dominates the interaction of the two oscillators in the monoclinic unit cell and determines the frequency splitting. For the other cases quadrupole–quadrupole or higher multipole interactions were found to be responsible for the splitting. Our model accounts almost quantitatively for the observed line positions and splittings in D_{2d}-$M_2@C_{84}$ dimetallofullerenes. The temperature dependence of the metal-cage vibrational structure implied a monoclinic crystal structure up to a temperature of at least 550 K. At approximately 150 K a phase transition from a disordered to an ordered orientational state is proposed.

II. EXPERIMENTAL AND THEORETICAL APPROACH

A. Sample preparation and Raman measurements

The empty D_{2d}-C_{84} fullerene and the D_{2d}-$M_2@C_{84}$ (M=Sc,Y,Dy) dimetallofullerene samples were prepared by a modified Krätschmer–Huffman arc burning method and subsequently soxhlet extracted in CS_2. For separation a multistage high performance liquid chromatography (HPLC) protocol described previously[15–17] was used. In all cases a final sample purity of at least 98% was obtained as established by HPLC and mass spectrometry.

For Raman studies solutions of $\approx$100 μg sample in 1 ml toluene were used to dropcoat gold covered silicon substrates at temperatures of about 50 °C. Samples were transferred into a liquid nitrogen (LN_2) cryostat and kept at a dynamic vacuum of $\sim 5\times10^{-7}$ mbar. For excitation of Raman scattering either the 514.5 nm Ar^+ line or the 647.1 nm Kr^+ line of a mixed gas ion laser model 2018 (Spectra Physics Corp., USA) were used. A prism premonochromator and adopted interference filters were applied to remove the plasma lines from the incident laser radiation. To reduce local heating a cylinder lens was inserted to spread the laser beam to a line focus of 0.05×2.0 mm^2. Raman spectra were recorded on a Dilor XY 500 spectrometer in the subtractive mode using a standard CCD detector. The spectral resolution was set to 2.0 cm^{-1} for the green and 1.5 cm^{-1} for the red laser wavelength, respectively. Temperature dependent spectra were recorded between 32 K and 550 K with a 20–25 K step width.

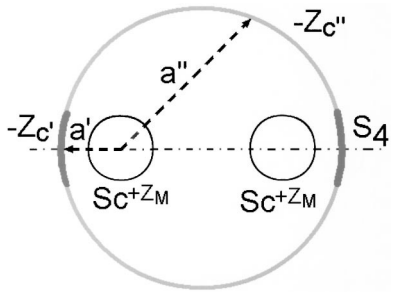

FIG. 1. Schematic view on the parameters used in the dynamical model for D_{2d}-$M_2@C_{84}$ crystals; Z_M, $Z_{C'}$, and $Z_{C''}$ represent the charges for the metal and the carbon atoms, a' and a'' are Born–Mayer parameters for two differently charged carbon atoms, S_4 depicts the molecular main symmetry axis.

B. The dynamical model

In order to estimate the factor-group and crystal-field splittings of the metal-cage modes quantitatively, calculations of the vibrational modes of $M_2@C_{84}$ crystals were carried out by means of a valence force field model.[18] The valence force field parameters for the C_{84} cage were transferred from graphite.[19] The *ab initio* electronic structure calculations by Nagase[20] revealed that the Sc–C bonding is mostly electrostatic. Moreover, neither significant positive overlap nor bond order was found between Sc and C. For these reasons, electrostatic interactions were accounted for between the encaged metal atoms and the carbon cage. Two Coulomb potentials were used between the metal atoms (with charge Z_M) and two classes of carbon atoms: the 2×2 nearest double bond carbon atoms (with charge $Z_{C'}$) on the one side and the 80 remaining carbons (with charge $Z_{C''}$) on the other side. In addition two different Born–Mayer potentials of the form $V(r)=a\exp(-br)$ were used where r is the metal-carbon distance and a and b represent the Born–Mayer parameters. No repulsive interactions were included between the different cages. A schematic drawing of the intramolecular forces is depicted exemplary for $Sc_2@C_{84}$ in Fig. 1. We note that the Born–Mayer potentials have essential short-range character whereas the longe-range Coulomb potentials are mainly responsible for the crystal forces. The orientational angles of the molecular S_4 symmetry axis and the values of the six disposable model parameters were derived by minimization of the interaction energy between the various atoms in the unit cell and by fitting to the observed Raman shifts. The condition for vanishing of the forces on the metal atoms was imposed during the minimization procedure. Using the obtained model parameters similar calculations were carried out for linear chains with one and two $Y_2@C_{84}$ molecules in the unit cell.

III. RESULTS

A. Vibrational analysis for D_{2d}-$M_2@C_{84}$ molecules

Based on ^{13}C-NMR spectroscopy[15,21] C_{84} and $Sc_2@C_{84}$ under study were assigned to the D_{2d}-C_{84} cage isomer 23 according to the fullerene nomenclature introduced by Fowler *et al.*[7] The isomers of $Y_2@C_{84}$ and $Dy_2@C_{84}$ under study have been attributed to the same D_{2d}-C_{84} cage due to

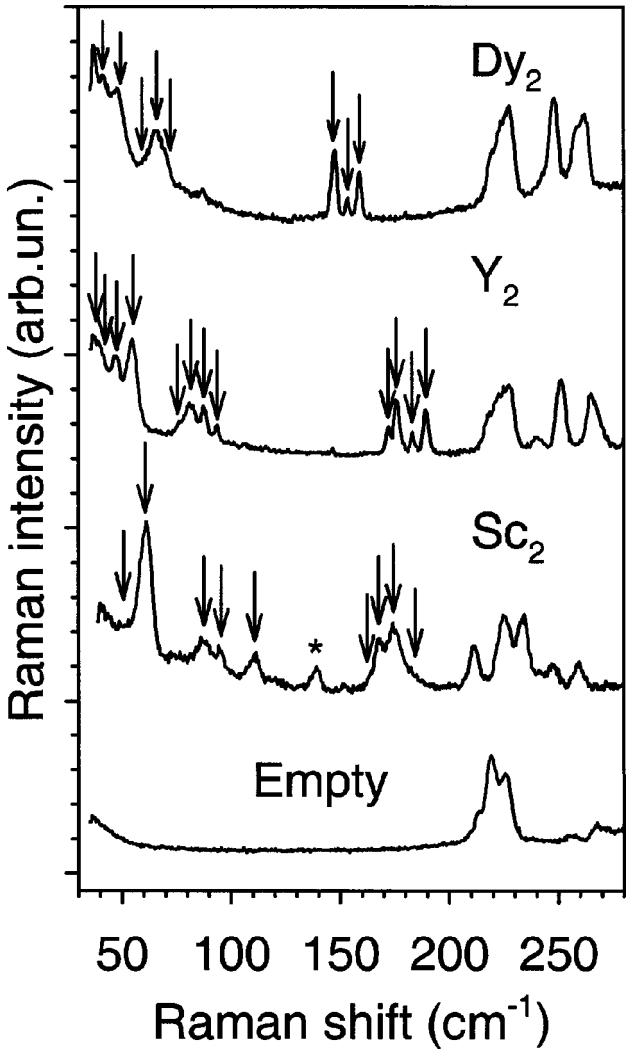

FIG. 2. Low energy Raman spectra of empty D_{2d}-C_{84} and D_{2d}-M_2@C_{84} (M=Sc,Y,Dy) at 100 K, 647 nm laser excitation, 2 (C_{84}) and 5 mW laser power, 1.5 cm^{-1} spectral bandpass, 2 h integration time per spectral window, M_2-C_{84} fundamentals are marked by arrows, * denotes a Sc_2-C_{84} line which is probably due to a Fermi resonance.

almost identical HPLC retention times and identical Vis-NIR spectra in comparison to the D_{2d}-Sc_2@C_{84} isomer.[16,17] The 246 vibrational degrees of freedom of the carbon cage are distributed on the irreducible representations of D_{2d} as

$$\Gamma_{\mathrm{vib},D_{2d}\text{-}C_{84}} = 32A_1(\mathrm{Ra}) + 30A_2(-) + 31B_1(\mathrm{Ra}) + 31B_2(\mathrm{Ra,IR}) + 61E(\mathrm{Ra,IR}). \quad (1)$$

From x-ray analysis is known that the Sc atoms in D_{2d}-Sc_2@C_{84} are accommodated on the fourfold inversion axis (S_4) of the C_{84} cage. Thus the overall D_{2d} molecular symmetry is retained for the dimetallofullerene.[22] Implying the same energetically favorable metal positions for D_{2d}-Y_2@C_{84} and -Dy_2@C_{84}, the group theoretical analysis for the free M_2@C_{84} molecules leads to four metal-cage modes with the following symmetry species:

$$\Gamma_{\mathrm{vib},M_2\text{-}C_{84}} = 1A_1(\mathrm{Ra}) + 1B_2(\mathrm{Ra,IR}) + 2E(\mathrm{Ra,IR}). \quad (2)$$

Raman (Ra) and infrared activities (IR) are given in parentheses. The A_1 and B_2 modes are metal-cage vibrations along the molecular S_4 axis with a distinct bond-stretching character. The E modes correspond to metal displacements perpendicular to the S_4 axis. In Ref. 9 these modes were assigned as lateral metal modes. Here we prefer the term metal-cage deformation vibrations.

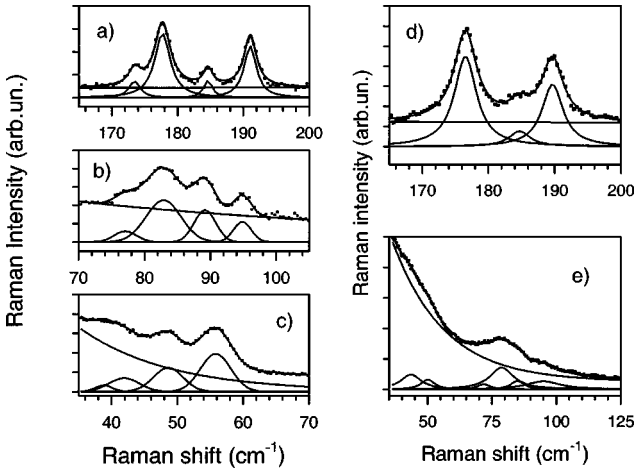

FIG. 3. Lorentzian line shape analysis for the metal-cage Raman lines of D_{2d}-Y_2@C_{84} at 100 K (a–c) and 300 K (d, e), recording parameters as in Fig. 2.

B. Metal and temperature dependent Raman spectra

Low energy Raman spectra of empty D_{2d}-C_{84} and D_{2d}-M_2@C_{84} dimetallofullerenes recorded at 100 K are presented in Fig. 2. The response of the empty cage is dominated by a line group with a center of gravity at 219 cm^{-1}. Weak lines appeared at 255 and 270 cm^{-1}. No Raman lines were detected below 200 cm^{-1}. A detailed line shape analysis revealed seven Raman lines for the empty C_{84} fullerene and as well as for the dimetallofullerenes in the range between 200 and 280 cm^{-1}. The five lower energetic dimetallofullerene lines correspond to the modes observed around 219 cm^{-1} for empty C_{84}. Their center of gravity is uniformly upshifted to 232 cm^{-1} in comparison to the unfilled carbon cage. For Sc_2@C_{84}, e.g., five Lorentzian lines at 211, 225, 233, 241, and 248 cm^{-1} account for the experimental profile. The spectral structure around 260 cm^{-1} is attributed to the superposition of the weak cage lines at 255 and 270 cm^{-1}. Neither additional lines nor metal dependent frequency shifts were found in the dimetallofullerene spectra between 200 and 280 cm^{-1} in comparison to empty D_{2d}-C_{84}. Thus all Raman lines in this range were assigned to cage modes.

Below 200 cm^{-1} the dimetallofullerenes exhibited a set of new Raman lines compared to empty C_{84}. For easier recognition these lines were marked by arrows in Fig. 2. Due to their absence in the Raman spectrum of the unfilled fullerene they are assigned to metal-cage modes, abbreviated as M_2-C_{84} modes in the following text. The M_2-C_{84} lines are not randomly distributed but exhibit a clusterlike spectral pattern of three line groups, labeled as I, II, and III in the order of increasing frequencies. Each of the groups consists of up to four lines. This is demonstrated for Y_2@C_{84} in Fig. 3: 12 Y_2-C_{84} lines were found at 100 K, and nine lines could be resolved at 300 K. For Dy_2@C_{84} and Sc_2@C_{84} a

TABLE I. Experimental (100 K and 300 K) and calculated frequencies of the metal-cage modes of $M_2@C_{84}$ crystals (in cm^{-1}). In addition the calculated frequencies of the isolated molecules are given in brackets. The symbols (*s*) and (*a*) stand for "symmetric" and "antisymmetric," respectively. The "h" means hidden by the elastic stray light.

	Deformation modes symmetric (group I)			Deformation modes antisymmetric (group II)			Stretching modes (group III)		
Sample	Expt. 100 K	300 K	Calc.	Expt. 100 K	300 K	Calc.	Expt. 100 K	300 K	Calc.
$Sc_2@C_{84}$			(54)			(104)			(171(*a*)) (181(*s*))
	48	*h*	51	84	77	96	164	···	167(*a*)
	48	*h*	53	88	···	98	168	165	172(*a*)
	58	*h*	54	95	91	99	175	175	181(*s*)
	61	51	59	110	106	103	180	175	181(*s*)
$Y_2@C_{84}$			(40)			(102)			(175(*s*)) (188(*a*))
	39	*h*	36	77	72	93	173	177	175(*s*)
	42	*h*	38	83	79	96	178	177	175(*s*)
	48	43	39	89	85	97	185	185	183(*a*)
	56	50	46	95	95	101	191	190	189(*a*)
$Dy_2@C_{84}$			(32)			(83)			(142(*s*)) (157(*a*))
	h	*h*	30	60	59	76	147	147	142(*s*)
	h	*h*	31	65	59	79	147	147	142(*s*)
	42	*h*	32	70	64	79	154	154	155(*a*)
	48	*h*	36	87	84	82	159	158	158(*a*)

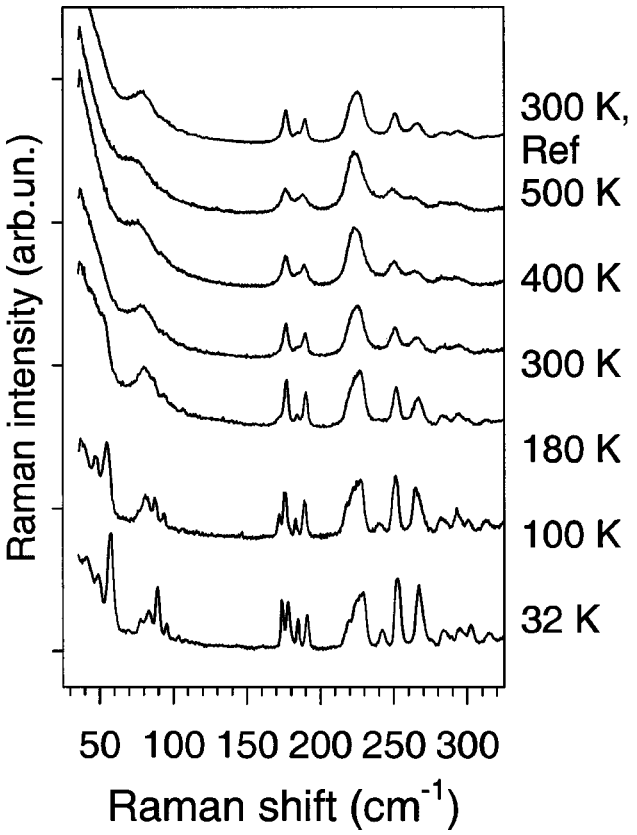

FIG. 4. Temperature dependent low energy Raman spectra of D_{2d}-$Y_2@C_{84}$, recording parameters as in Fig. 2.

similar number of M_2-C_{84} modes was observed. The complete data are listed in Table I. Two missing components of the Dy_2-C_{84} line group I are hidden by the elastic scattering light. The M_2-C_{84} lines displayed significant metal dependent frequency shifts. This is a second experimental proof for a metal based origin. Correlation coefficients of $R^2=0.995$ and $R^2=0.993$ were obtained for the average frequency of group II and two highest components of the M_2-C_{84} mode group I with respect to the square root of the reciprocal reduced mass of an idealized superatomic M_2-C_{84} molecule. On the other hand the frequencies of the highest energetic metal induced line group III did not show such a linear correlation but had a maximum value for $Y_2@C_{84}$ with the intermediate metal mass.

To get insight into dynamic properties of D_{2d}-$Y_2@C_{84}$ dimetallofullerenes the temperature dependence of the Raman response was studied in detail. The measurements were started at 300 K without prior sample heating. Hence, residing toluene was presumably present, similar as in the x-ray study of Takata *et al.*[22] The low temperature response down to 32 K was studied next. During the final high temperature studies up to 550 K repeated reference measurements at 300 K were used to check for spectral changes due to toluene evaporation or a possible thermal degradation of the sample. Representative temperature dependent low energy Raman spectra are shown in Fig. 4. The Raman response of $Y_2@C_{84}$ can be classified into two temperature regions:

(i) 550–180 K,
(ii) 180–32 K.

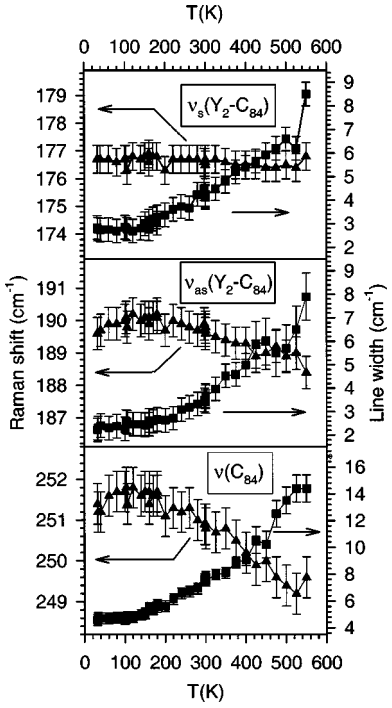

FIG. 5. Temperature dependence of frequency and linewidths for selected D_{2d}-$Y_2@C_{84}$ Raman modes; assignments according to Table I.

In the high temperature range the Y_2-C_{84} line group III consists of three components, the four lines of the group II are broad and overlap, and the group I is partially hidden by the elastic stray light. This spectral signature is independent from the presence of solvent molecules, which are completely removed at 475 K.[12] Neither a significant influence of solvent on line positions or widths was found. Starting at 180 K down to 32 K continuous spectral changes were observed. A fourth component appeared on the low frequency side of Y_2-C_{84} line group III and gained intensity with decreasing temperature. Similarly one component from the Y_2-C_{84} line groups I and II became dominant at very low temperatures.

The detailed frequency and line width evolution of three selected $Y_2@C_{84}$ Raman lines is displayed in Fig. 5. Selection criteria were an undistorted line profile in the whole temperature range on the one hand and the inclusion of Y_2-C_{84} and C_{84} cage lines on the other hand. No discontinuous changes were found in the whole temperature range. Two of the lines exhibited a shallow frequency maximum around 120 K. Temperature induced frequency shifts of $\leqslant 0.7$ cm^{-1}/100 K were found for the majority of Raman lines. Larger shifts were observed for the lower energetic Y_2-C_{84} line groups: 1.6 cm^{-1}/100 K for the averaged group II frequency and even 2.5 and 3.0 cm^{-1}/100 K for the lines of group I. The linewidths were in general almost constant from 32 K to around 140 K. From 150 K onwards they showed an activation like broadening up to 550 K. Similar results as for $Y_2@C_{84}$ were obtained for $Dy_2@C_{84}$ and $Sc_2@C_{84}$ (Table I).

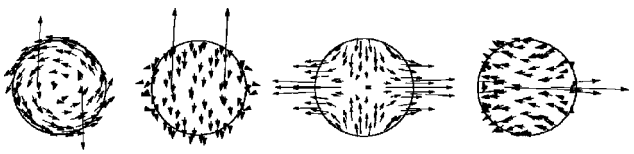

FIG. 6. Atomic displacements of the metal-cage vibrations in D_{2d}-$Y_2@C_{84}$ molecules: symmetric deformation, antisymmetric deformation, symmetric stretching, and antisymmetric stretching vibration (from left to right).

C. Assignment of metal-cage modes in D_{2d}-$M_2@C_{84}$ dimetallofullerene crystals

To assign the observed M_2-C_{84} Raman lines to specific vibrational modes and to understand the forces which are responsible for the observed splitting a dynamical model described in Sec. II B was applied. In Table I calculated frequencies for $M_2@C_{84}$ molecules and crystals are listed in comparison to our experimental results. In Fig. 6 atomic displacements are presented for the four M_2-C_{84} molecular vibrations. The observed pattern of three M_2-C_{84} line groups was quantitatively confirmed by the calculation. The lines of group III are assigned to antisymmetric and symmetric stretching vibrations. The group II modes are antisymmetric deformation modes, where the metal ions are vibrating perpendicular to the S_4 axis with opposite phase. Finally, the metal-cage modes of group I are assigned to in phase metal displacements perpendicular to S_4, i.e., symmetric deformation modes. The calculated frequencies of the M_2-C_{84} stretching modes agree within $\Delta\tilde{\nu}=+2.5$ *to* -3.5% compared to the experimental data. Deviations of $\Delta\tilde{\nu}=+5$ *to* $+13\%$ and $\Delta\tilde{\nu}=0$ *to* -14% were obtained for the antisymmetric and symmetric deformation modes. Nevertheless their assignment is unambiguous as interferences with other modes are to be excluded. Based on the present work a previous tentative assignment for the symmetric Sc_2-C_{84} stretching mode in Ref. 13 could be specified. In a recent theoretical work on D_{2d}-$Sc_2@C_{84}$ molecules wave numbers of 215, 216, 138, and 94 cm^{-1} were predicted for the Sc_2-C_{84} modes.[23] Whereas the mode ordering and sequence in Ref. 23 agree very well with our results, the frequencies exhibit an average offset of 43 cm^{-1} compared to our data. Frequency offsets are intrinsic properties of quantumchemical calculations, which are in general treated by the introduction of specific scaling factors. As very similar frequency offsets were found for the four Sc_2-C_{84} modes, scaling seems to be appropriate to reduce the difference between the present and the results in Ref. 23.

For the spectrum of $Sc_2@C_{84}$ one line at 138 cm^{-1} remains unexplained so far. Its assignment to one component of the antisymmetric deformation mode would infer a crystal field splitting of 40 cm^{-1} which is very unusual and does not correspond to the calculated values. A possible explanation is the response from the overtone of the symmetric deformation mode at 62 cm^{-1}, enhanced and up-shifted by a Fermi resonance with the highest component of the antisymmetric deformation mode.

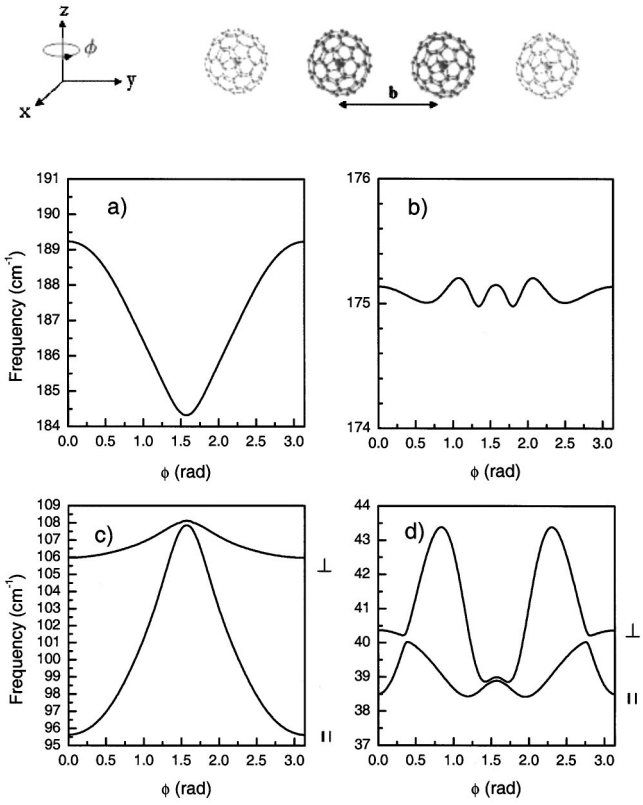

FIG. 7. Splitting of the metal-cage modes of $M_2@C_{84}$ in a linear chain with one molecule per unit cell vs the angle φ of the S_4 axis with respect to the chain. The four panels present results for (a) antisymmetric stretching, (b) symmetric stretching, (c) antisymmetric deformation, and (d) symmetric deformation modes. The symbols $\perp$ and $\parallel$ stand for movements perpendicular and parallel to the chain.

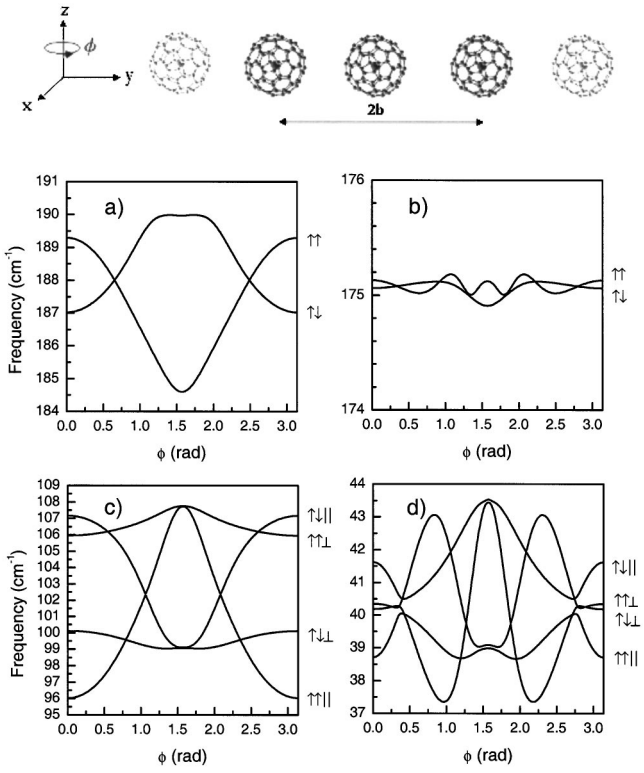

FIG. 8. Splitting of the metal-cage modes of $M_2@C_{84}$ in a linear chain with two molecules per unit cell vs the angle φ of the S_4 axis with respect to the chain. The four panels present results for (a) antisymmetric stretching, (b) symmetric stretching, (c) antisymmetric deformation, and (d) symmetric deformation modes. The notations $\uparrow\uparrow$ and $\uparrow\downarrow$ designate modes with in-phase and counter-phase motion of the metal atoms in the two molecules. The symbols $\perp$ and $\parallel$ have the same meaning as for Fig. 7.

IV. DISCUSSION

A. Crystal field splitting of metal-cage vibrations

According to Eq. (2) four metal-cage vibrational modes are expected for D_{2d}-$M_2@C_{84}$ molecules. Hence, the molecular approach is not sufficient to explain the observed number of metal-cage Raman lines of D_{2d}-$M_2@C_{84}$ (M = Sy, Y,Dy) dimetallofullerene crystals. In addition, the crystal structure has to be taken into account. $Sc_2@C_{84}$ crystallizes in space group $P2_1$.[22] This monoclinic space group and moreover specific lattice parameters $\mathbf{b_0}=\mathbf{c_0}$ and $\beta\approx 108°$ were found for numerous empty and filled fullerene crystals grown from toluene.[24–26] Due to the identity of the carbon cage isomers, the presence of the same solvent during crystallization as in Ref. 22, and the same high degree of M_2-C_{84} mode splitting, this space group was adopted for the further analysis of the observed Raman response. The space group $P2_1$ has only one set of two $a1$ sites, i.e., the basis of the primitive unit cell consists of two molecules which occupy sites of symmetry 1 (C_1). As a result of the low site symmetry, the crystal field splits the 2 E modes into two components of symmetry A. The 2 M_2-C_{84} stretching modes are likewise correlated to this site symmetry species. Additionally, the interaction of the two molecules in the unit cell gives rise to factor-group splitting yielding modes of A and B symmetry species for each crystal field component.[13] The total number of metal-cage modes will be 12: eight deformation modes, two symmetric and two antisymmetric stretching modes. Group theory entirely accounts for the experimental data. On the other hand the metal-cage modes of D_{2d}-C_{84} based dimetallofullerenes and in particular of D_{2d}-$Y_2@C_{84}$ are intriguing examples for a full crystal field and factor group splitting of a particular group of vibrational modes.

In order to understand the responsible forces for the observed crystal field splitting in D_{2d}-$M_2@C_{84}$ crystals model calculations for linear chains of dimetallofullerenes with one and two molecules per unit cell were performed as a function of a rotation angle φ. The angle φ is equal to zero for the perpendicular orientation of the molecular S_4 symmetry axis with respect to the chain axis and equal to $\pi/2$ for the parallel orientation. The results for the zone-center M_2-C_{84} phonons ($k=0$) are shown in Figs. 7 and 8. Apparently the frequencies and the number of resolvable lines depend significantly on the orientation of the $M_2@C_{84}$ molecules in the chain. For one molecule per unit cell, all molecules vibrate with the same phase (in-phase motion). The crystal field splits the doubly degenerated deformation modes into components with metal motions parallel and perpendicular to the chain (denoted by the symbols $\perp$ and $\parallel$ in Fig. 7). The angular dependence of the mode frequencies reveals the physical origin of the crystal field effects. For the antisymmetric stretching and deformation modes the frequencies exhibit an angular dependence of $V_\mu \propto 1-3\cos^2\varphi$, what corresponds to the interaction of dipoles arranged in a linear chain. As the

TABLE II. Model parameters used for the calculation of the metal-cage modes in molecular and crystaline $M_2@C_{84}$ compounds. The charge is given in units of the elementary charge, a and b are in eV, and $Å^{-1}$, respectively.

	Ionic charges			Born–Mayer parameters		
Metal atom	Z_M	$Z_{C'}$	$Z_{C''}$	a'	a''	b
Sc	1.60	−0.20	−0.03	520	694	3.464
Y	2.20	−0.30	−0.04	1345	2403	3.505
Dy	2.20	−0.30	−0.04	1312	2344	3.420

D_{2d}-$M_2@C_{84}$ molecules have no permanent dipole moment, vibration induced dipole–dipole interactions are responsible for this behavior. The angular dependence of the symmetric modes is smaller than of the antisymmetric modes and in general for more complex. It corresponds basically to the angular dependence of a quadrupole–quadrupole interaction, according to $V_\Theta \propto 3-30\cos^2\varphi+25\cos^4\varphi$. Contributions of higher multipole interactions give rise to minor deviations from the ideal quadrupole–quadrupole angular dependence. The difference in the distance dependence of dipole–dipole ($V_\mu \propto 1/r^3$) and quadrupole–quadrupole interactions ($V_\Theta \propto 1/r^5$) accounts for the larger effect of the former type of crystal field interactions on the M_2-C_{84} frequencies and splitting energies. For a dimolecular chain, the interaction between the molecules in the unit cell leads to factor group or Davydov splitting. From each mode of the monomolecular chain originate two modes with in-phase and antiphase motion (denoted by $\uparrow\downarrow$) of the metal atoms in the two molecules of the unit cell as shown in Fig. 8. Depending on the rotation angle φ a factor group splitting of $2.5\ \mathrm{cm}^{-1} \leqslant \Delta\tilde{\nu} \leqslant 5.5\ \mathrm{cm}^{-1}$ was calculated for the antisymmetric Y_2-C_{84} stretching mode, what is in the same order as the observed splittings in dimetallofullerene crystals. The predicted small splitting of $\sim 0.2\ \mathrm{cm}^{-1}$ for the symmetric stretching mode precludes their observation as two separate peaks in the Raman spectrum in the temperature range from 180 K to 550 K. Moreover, the model calculation reproduced the larger crystal field splitting of the M_2-C_{84} deformations modes compared to the stretching vibrations.

The model parameters accounting for the observed Raman frequencies in $M_2@C_{84}$ crystals are given in Table II. The Born–Mayer parameters as well as the Coulomb charges are nearly identical for D_{2d}-$Y_2@C_{84}$ and -$Dy_2@C_{84}$, but somewhat different for $Sc_2@C_{84}$. They imply stronger short-range metal–carbon interactions and a larger charge transfer in the former dimetallofullerenes compared to the Sc_2 compound. The weaker metal-cage interaction in $Sc_2@C_{84}$ accounts for the unexpected low value of the Sc_2-C_{84} stretching frequencies compared to the yttrium and dysprosium dimetallofullerenes. It has to be noted, that the metal-cage stretching frequencies reflect the superposition of ionic, covalent, and crystal field contributions to the overall metal-cage bond energy. Whereas a reliable bond strength ordering is obtained, our approach does not provide a direct measure of the transferred charge.

B. Molecular and lattice dynamics of D_{2d}-$M_2@C_{84}$ dimetallofullerenes

The temperature dependence of the M_2-C_{84} deformation mode frequencies is significantly higher than those of C_{84} cage modes and M_2-C_{84} stretching modes: 1.6–5.0 cm^{-1}/100 K compared to 0–0.7 cm^{-1}/100 K. For intramolecular vibrations in molecular crystals line shifts up to 1 cm^{-1}/100 K are common. Larger shifts are typical for lattice phonons. Their larger temperature dependence implies a stronger interaction of M_2-C_{84} deformation modes with the crystal lattice than it is the case for the C_{84} cage and the M_2-C_{84} stretching modes. Such a coupling could involve lattice phonons or cage rotations.

The kink in the widths of the $Y_2@C_{84}$ Raman lines around 150 K indicates another dynamic process. Below this temperature the linewidths remained almost constant. This observation represents an intrinsic property of the vibrational modes, as the linewidths of ν_{as} (Y_2-C_{84}), ν_s (Y_2-C_{84}), and the C_{84} cage mode at 250 cm^{-1} are well beyond the resolution of the spectrometer. Apparently one relaxation channel is no more available below 150 K. In C_{60} crystals beyond the phase transition from sc to fcc at 255 K the molecules are rotating almost free, i.e., with random orientation. Below this temperature the C_{60} molecules rotate in a few locked orientations and the basis of the spectroscopic unit cell increases from one to four molecules. This phase transition causes steps and kinks in the temperature evolution of C_{60} vibrational line widths as well as a line splitting.[27] Two factors account for a lower order–disorder phase transition temperature in $Y_2@C_{84}$: On the one hand the moment of inertia I is roughly by a factor 2 larger than for C_{60}. As $E_{rot} \propto 1/I$, less energy is necessary to excite cage rotations. On the other hand, the energy gain due to favorable alignments of cage double bonds and hexagons in the ordered phase should be of the same order or even smaller for larger carbon cages than C_{60}. Hence, the observed linewidth evolution is attributed to a transition from an ordered to a rotationally disordered state of $Y_2@C_{84}$ around 150 K. A similar phase transition was reported for D_{2d}-$Sc_2@C_{84}$ at 160 K.[28]

Below the transition temperatures, a fourth M_2-C_{84} stretching vibration was observed for the Y_2 and the Sc_2 compound. This line is not predicted by our dynamical model, neither for the dimetallofullerene crystals nor for the two linear chain models. A careful inspection of the low temperature phase $Y_2@C_{84}$ Raman spectrum in Fig. 4 reveals at least three more lines of weak intensity at 70, 104, and 108 cm^{-1}. As the number of 12 M_2-C_{84} cage modes allowed for space group $P2_1$ is exceeded, our data infer a larger spectroscopic unit cell in the low temperature phase.

Solvent grown crystals of empty fullerenes like C_{76} and C_{82} crystallized in space group $P2_1$ were reported to undergo a structural phase transition from a monoclinic to a fcc lattice at temperatures around 375 K due to the loss of the solvent.[24] As the Y_2-C_{84} vibrational structure in general and in particular the number of three Y_2-C_{84} stretching modes did not change during sample heating (see Fig. 4), such a transition can be excluded for D_{2d}-$Y_2@C_{84}$ dimetallofullerene up to temperatures of 550 K. The higher thermal stability of the monoclinic crystal structure is presumably due to electro-

static interactions of the molecular dimetallofullerene quadrupoles in the crystal, which make a rearrangement to a cubic structure more difficult.

V. SUMMARY

In conclusion, agreement between calculation and experiment for metal-cage vibrational modes in D_{2d}-M_2@C_{84} dimetallofullerene crystals has been demonstrated. The present study provides for the first time a quantitative description of crystal-field and factor-group splitting in these systems. The M_2-C_{84} modes exhibit a full crystal field induced splitting of molecular vibrations according to group theoretical predictions. The physical origin for the splitting are static and dynamic dipole and quadrupole interactions. These interactions account further for the unusual high thermal stability of the monoclinic crystal structure of D_{2d}-Y_2@C_{84} dimetallofullerene. Lateral, M_2-C_{84} deformation modes of D_{2d}-M_2@C_{84} dimetallofullerenes show a stronger coupling to the crystal lattice than pure C_{84} cage modes and M_2-C_{84} stretching vibrations. At a temperature of approximately 150 K Y_2@C_{84} dimetallofullerene undergoes a phase transition from a disordered to an ordered orientational state.

ACKNOWLEDGMENTS

The submission of Sc_2@C_{84} crystal data from Dr. Nishibori is cordially acknowledged. We also acknowledge financial support from the European Union, TMR project Fulprop, ERBFMRX-CT97-0155. P. G. thanks the Deutsche Forschungsgemeinschaft, Project No. DU 225/13-2 for founding.

[1] J. Heath, S. C. O'Brien, Q. Zhang, Y. Liu, R. F. Curl, H. W. Kroto, F. K. Tittel, and R. E. Smalley, J. Am. Chem. Soc. **107**, 7779 (1985).
[2] H. Shinohara, Rep. Prog. Phys. **63**, 843 (2000).
[3] M. Saunders, R. J. Cross, H. A. Jimenez-Vazquez, R. Shimshi, and A. Khong, Science **271**, 1693 (1996).
[4] T. Almeida-Murphy, T. Pawlik, A. Weidinger, M. Höhne, R. Alcala, and J.-M. Spaeth, Phys. Rev. Lett. **77**, 1075 (1996).
[5] S. Stevenson, G. Rice, T. Glass, K. Harich, F. Cromer, M. R. Jordan, J. Craft, E. Hajdu, R. Bible, M. M. Olmstead, K. Maitra, A. J. Fisher, A. L. Balch, and H. C. Dorn, Nature (London) **401**, 55 (1999).
[6] C. Wang, T. Kai, T. Tomiyama, T. Yoshida, Y. Kobayashi, E. Nishibori, M. Takata, M. Sakata, and H. Shinohara, Angew. Chem. **113**, 411 (2001).
[7] P. W. Fowler and D. E. Manolopoulos, *An Atlas of Fullerenes* (Clarendon, Oxford, 1995).
[8] M. S. Dresselhaus, G. Dresselhaus, and P. C. Eklund, *Science of Fullerenes and Carbon Nanotubes* (Academic, San Diego, 1996), and references cited therein.
[9] S. Lebedkin, B. Renker, R. Heid, H. Schober, and H. Rietschel, Appl. Phys. A: Mater. Sci. Process. **66**, 273 (1998).
[10] M. Krause, P. Kuran, U. Kirbach, and L. Dunsch, Carbon **37**, 113 (1999).
[11] P. Kuran, M. Krause, A. Bartl, and L. Dunsch, Chem. Phys. Lett. **292**, 580 (1998).
[12] M. Krause and H. Kuzmany, in *Endofullerenes: A New Family of Carbon Clusters*, edited by T. Akasaka and S. Nagase (Kluwer Academic, Dordrecht, 2002), pp. 169–184.
[13] M. Krause, M. Hulman, H. Kuzmany, T. J. S. Dennis, M. Inakuma, and H. Shinohara, J. Chem. Phys. **111**, 7976 (1999).
[14] M. Krause, H. Kuzmany, P. Georgi, L. Dunsch, K. Vietze, and G. Seifert, J. Chem. Phys. **115**, 6596 (2001).
[15] E. Yamamoto, M. Tansho, T. Tomiyama, H. Shinohara, H. Kawahara, and Y. Kobayashi, J. Am. Chem. Soc. **118**, 2293 (1996).
[16] P. Kuran, "Über neuartige dimetallofullerene und fullerene mit kleinerem Käfig," Ph.D. thesis, Dresden, 2002.
[17] N. Tagmatarchis and H. Shinohara, Chem. Mater. **12**, 3222 (2000).
[18] G. Turrell, *Infrared and Raman Spectra of Crystals* (Academic, London, 1972).
[19] T. Aizawa, R. Souda, S. Otani, Y. Ishizawa, and C. Oshima, Phys. Rev. B **42**, 11469 (1990).
[20] S. Nagase and K. Kobayashi, Chem. Phys. Lett. **231**, 319 (1994).
[21] K. Kikuchi, N. Nakahara, T. Wakabayashi, M. Honda, H. Matsumiya, T. Moriwaki, S. Suzuki, H. Shiromaru, K. Saito, K. Yamauchi, I. Ikemoto, and Y. Achiba, Chem. Phys. Lett. **188**, 177 (1992).
[22] M. Takata, E. Nishibori, B. Umeda, M. Sakata, E. Yamamoto, and H. Shinohara, Phys. Rev. Lett. **78**, 3330 (1997).
[23] K. Kobayashi and S. Nagase, Mol. Phys. **101**, 249 (2003).
[24] H. Kawada, Y. Fujii, H. Nakao, Y. Murakami, T. Watanuki, H. Suematsu, K. Kikuchi, Y. Achiba, and I. Ikemoto, Phys. Rev. B **51**, 8723 (1995).
[25] M. Takata, B. Umeda, E. Nishibori, M. Sakata, Y. Saito, M. Ohno, and H. Shinohara, Nature (London) **377**, 46 (1995).
[26] E. Nishibori, M. Takata, M. Sakata, M. Inakuma, and H. Shinohara, Chem. Phys. Lett. **298**, 79 (1998).
[27] R. Winkler, T. Pichler, and H. Kuzmany, Z. Phys. B: Condens. Matter **96**, 39 (1994).
[28] M. Inakuma, E. Yamamoto, T. Kai *et al.*, J. Phys. Chem. B **104**, 5072 (2000).